

CapsuleBot: A Novel Compact Hybrid Aerial-Ground Robot with Two Actuated-wheel-rotors

Zhi Zheng ^{† 1,2,3}, Qifeng Cai ^{† 1,2,3}, Xinhang Xu ⁴, Muqing Cao ⁴,
Huan Yu ^{1,2,3}, Jihao Li ^{1,2,3}, Guodong Lu ^{1,2,3}, and Jin Wang^{1,2,3}

Abstract—This paper presents the design, modeling, and experimental validation of CapsuleBot, a compact hybrid aerial-ground vehicle designed for long-term covert reconnaissance. CapsuleBot combines the manoeuvrability of bicopter in the air with the energy efficiency and noise reduction of ground vehicles on the ground. To accomplish this, a structure named actuated-wheel-rotor has been designed, utilizing a sole motor for both the unilateral rotor tilting in the bicopter configuration and the wheel movement in ground mode. CapsuleBot comes equipped with two of these structures, enabling it to attain hybrid aerial-ground propulsion with just four motors. Importantly, the decoupling of motion modes is achieved without the need for additional drivers, enhancing the versatility and robustness of the system. Furthermore, we have designed the full dynamics and control for aerial and ground locomotion based on the bicopter model and the two-wheeled self-balancing vehicle model. The performance of CapsuleBot has been validated through experiments. The results demonstrate that CapsuleBot produces 40.53% less noise in ground mode and consumes 99.35% less energy, highlighting its potential for long-term covert reconnaissance applications.

I. INTRODUCTION

In recent years, although significant progress has been made in unmanned systems, particularly in unmanned ground vehicles (UGVs) and unmanned aerial vehicles (UAVs), across a range of industries including search and rescue, exploration, transportation, monitoring, and more, [1] [2] [3] [4] [5] the pursuit of excellence in design and complex applications is still ongoing.

In the field of covert reconnaissance, UGVs are highly regarded for their low noise, low energy consumption, and stable ground mobility, making them ideal for prolonged and extensive covert reconnaissance missions [6]. However, their limited ground movement capability and relatively large size restrict their delivery radius and prevent them from performing targeted landing sites during airdrops. Moreover, in environments characterized by extensive urban operations and battlefield ruins, UGVs face various uncertain obstacles that can significantly impede their vision and action, ultimately

This work was supported in part by the National Natural Science Foundation of China under Grant 52175032, the “Pioneer” and “Leading Goose” R&D Program of Zhejiang under Grant 2023C01070, and Robotics Institute of Zhejiang University under Grant K12107 and K11805.

[†] Equal contribution.

¹The State Key Laboratory of Fluid Power and Mechatronic Systems, School of Mechanical Engineering, Zhejiang University, Hangzhou 310027, China. ²Robotics Institute of Zhejiang University, Hangzhou 310027, China.

³Robotics Research Center of Yuyao City, Ningbo 315400, China. ⁴School of Electrical and Electronic Engineering, Nanyang Technological University, 50 Nanyang Avenue, Singapore.

Email: {z.z., dwjcom}@zju.edu.cn

Corresponding author: Jin Wang.

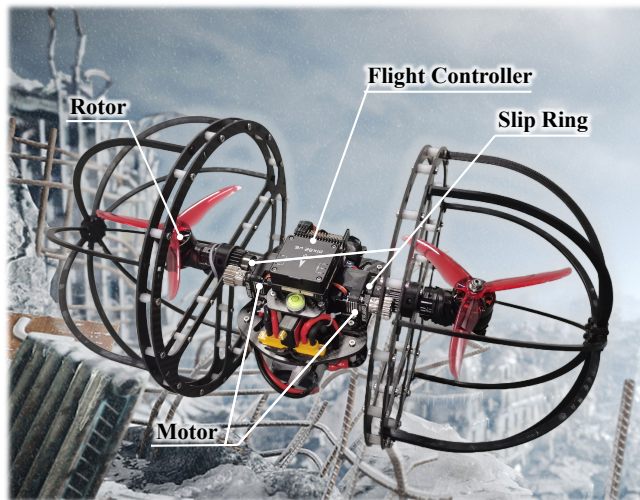


Fig. 1: Our CapsuleBot prototype.

reducing mission efficiency. In contrast, UAVs with flight capabilities exhibit excellent maneuverability in exploring unstructured and challenging environments [7]. They can rapidly reach target areas, provide aerial surveillance, overcome obstacles, and achieve comprehensive reconnaissance. However, UAVs are also constrained by payload capacity, flight time limitations, and susceptibility to collision damage. Additionally, they encounter difficulties in conducting covert reconnaissance over extended periods of time and maneuvering in narrow spaces.

Hybrid aerial-ground vehicles have been extensively studied as a potential solution for mobility in complex environments, as they can combine the advantages of flight and ground locomotion. However, there are limited solutions available that meet the aforementioned requirements. The use of propellers to drive the ground mode [8] [9] [10] results in significant noise and dust, while the coupling of movement modes often leads to poor system adaptability. Active terrestrial locomotion systems using walking [11] or climbing [12] have the ability to handle rough terrain at the cost of complex connections or slow movement. In this context, a vehicle structure with active wheels appears to be a more effective mechanical design. One simple solution is to mount the UGV directly under the UAV [13] [14], but this approach significantly reduces flight efficiency due to the additional load. Although there are challenges in the stable transitions between motion modes, some designs have successfully improved the integration of multi-modal

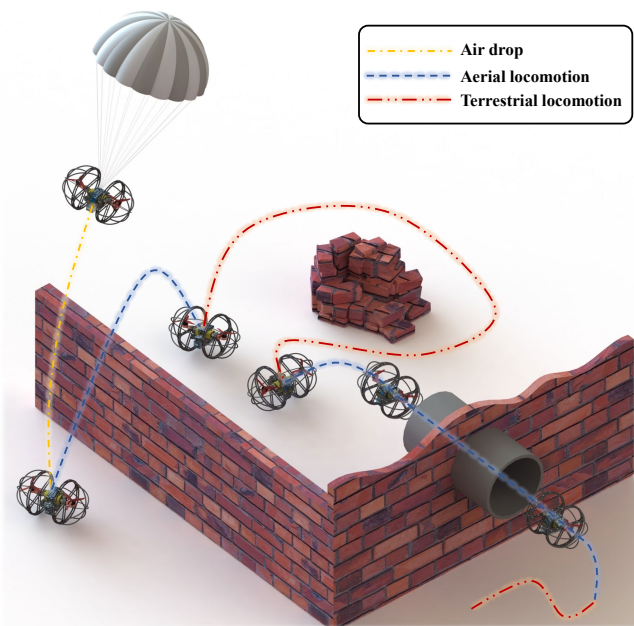


Fig. 2: An envisioned CapsuleBot application scenario. The robot can be deployed into a concealed reconnaissance area in either flying or rolling modes. The ground locomotion is generally preferred for long-term covert reconnaissance because of energy-saving and low-noise. The normal flight mode is used to fly over common obstacles, while the lateral flight mode allows the robot to navigate through pipes or narrow gaps.

vehicles and optimized the overall weight of the platform through fuselage deformation [15], reconstruction [16], and transformation [17]. These designs have also demonstrated better maneuverability in navigating through small openings.

In this paper, we present the design of a compact hybrid aerial-ground robot called CapsuleBot. The main objective of this robot is to perform covert reconnaissance missions for extended periods. To achieve this, we combine the aerial agility of a bicopter with the energy efficiency and noise reduction capabilities of a two-wheel self-balancing robot when it operates on the ground. This innovative design is based on the concept of actuated-wheel-rotor. By incorporating two of these structures, CapsuleBot is capable of achieving hybrid motion using only four motors. This not only enhances its versatility but also eliminates the need for additional drivers. Furthermore, we address the issue of wire winding during ground locomotion by implementing slip rings.

Compared to previous multi-rotor hybrid aerial-ground vehicles, CapsuleBot's actuated-wheel-rotor provides enhanced ground maneuverability. This design minimizes the risk of sensory degradation and body damage by eliminating the dusty generation caused by propeller whirling. Additionally, the smaller movement noise ensures that CapsuleBot can go undetected during covert reconnaissance missions. Furthermore, the compactness and energy efficiency of the bicopter make the robot particularly suitable for certain long-term

tasks, such as cave exploration and pipeline inspection. A bicopter consumes 30% less power than a quadrotor of the same weight and size [18], making it more efficient. The smaller radial size also allows the vehicle to roll through narrow gaps. Fig. 2 illustrates an envisioned search and reconnaissance example.

The comprehensive dynamics and control system, which incorporates models of both the bicopter and self-balancing robot, has been validated through experiments. These experiments have shown a significant 40.53% reduction in noise and an impressive 99.35% decrease in energy consumption during ground mode. These results demonstrate the effectiveness of CapsuleBot as a covert and persistent Intelligence, Surveillance, and Reconnaissance (ISR) platform. CapsuleBot is capable of loitering near a target for extended periods of time.

The main contributions of this paper are summarized as:

- A novel compact hybrid aerial-ground robot with two actuated wheel-rotors is proposed and built. This robot utilizes a single motor for both the unilateral rotor tilt in the bicopter configuration and the wheel motion in ground mode.
- Comprehensive dynamics modeling and controller design are conducted, encompassing both aerial and ground locomotion.
- Experimental results confirm the performance of CapsuleBot in different modes and demonstrate its high energy efficiency and low noise level in ground mode.
- Two challenging missions are conducted to demonstrate the capabilities of CapsuleBot in traversing regions with different types of obstacles.

II. MECHATRONIC SYSTEM DESIGN

A. System Architecture and Components

The composition of CapsuleBot is depicted in Fig. 3. The robot weighs about 1.5 kg. The robot's main body is designed with axial symmetry and constructed using a carbon fiber frame (Fig. 3 (5)). To enhance safety and aesthetics, a spherical propeller protector is incorporated (Fig. 3 (4)). This protector is made from 3D printed ABS material, known for its partial elasticity and ability to absorb impact energy, thereby protecting the robot from potential damage during impacts. The system is powered by a 3000 mAh 6s 75c battery (Fig. 3 (8)).

In flight mode, we utilize two motors (Fig. 3 (7)) to control the tilt of the rotors (Fig. 3 (1)) through gearing (Fig. 3 (6)), resulting in a bicopter configuration. To generate thrust, the vehicle is equipped with T-MOTOR F90 1500KV rotors and 6-inch three-blade propellers, which have a diameter of 26 cm. For flight control and electronic speed regulation, we employ the Holybro Pix32 v6 flight controller and FLYCOLOR 45A ESC (Fig. 3 (2)).

In ground mode, we utilize the same motors that are used to tilt the rotors (Fig. 3 (5)). These motors drive carbon fiber wheels with a diameter of 25 cm through gearing. This design choice aims to minimize energy consumption,

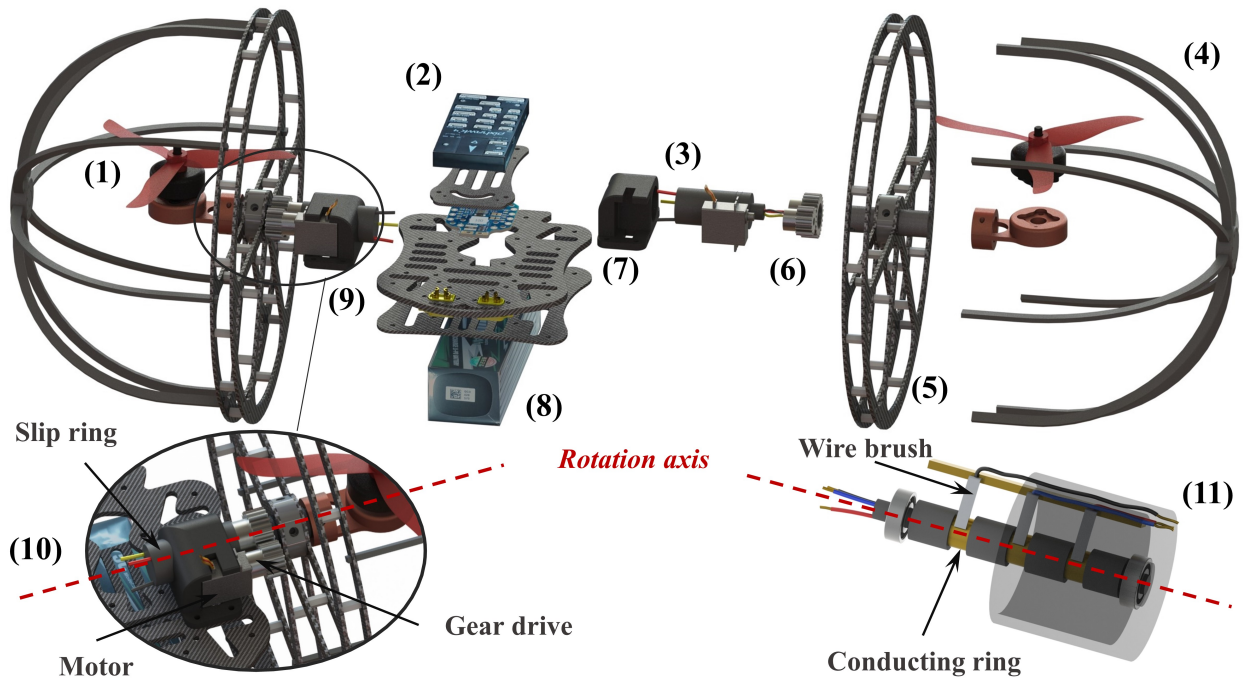


Fig. 3: The composition of CapsuleBot is detailed below. The serial numbers correspond to specific components: (1) rotor, (2) flight controller and electronic speed controller (ESC), (3) slip ring, (4) spherical propeller protector, (5) carbon fiber wheel, (6) gear drive, (7) motor, (8) battery, (9) carbon fiber frame, (10) gear transmission system design, and (11) slip ring design, which includes an installation diagram.

achieve low noise levels, and reduce the risk of sensory degradation and body damage caused by propeller erosion in dusty environments. The wheels are designed with two rigidly attached carbon fibre frames to ensure robustness and durability. Additionally, to address the issue of wire winding for the rotor during wheeled motion, we have incorporated slip rings (Fig. 3 (3) and (11)).

B. Drive and Transmission System Design

In flight mode, when the throttle valve is set at 55%, each rotor we have chosen can generate a thrust of 811 *g*. The current required for this operation is approximately 8.86 *A*. This level of performance not only satisfies the thrust requirements in this mode but also remains below the upper limits of both the ESC and slip ring in terms of current.

In ground mode, after the robot is activated, the motor rotates to generate torque based on the instructions provided by the flight controller. This torque is then transmitted through the gear transmission (Fig. 3(10)), with a transmission ratio of $i = 16 : 25$. It is important to note that the rotor only operates in flight mode and remains inactive in ground mode.

This approach enables our robot, CapsuleBot, to be designed in a compact manner and capable of both land and air movement, with low noise levels and reduced energy consumption. Through the effective combination of these mechanisms, the proposed CapsuleBot demonstrates significant potential for long-term covert reconnaissance applications.

III. MODELING AND CONTROL

A. Aerial Mode

1) *MODELING*: When CapsuleBot is in flight, there are no friction or contact forces acting on its wheels. As a result, the dynamics equations can be simplified to those of a standard bicopter [18]. The torque generated is produced by the rotor thrusts:

$$\begin{cases} \tau_x = (F_1 \cos \theta_1 - F_2 \cos \theta_2) D/2, \\ \tau_y = (F_1 \sin \theta_1 + F_2 \sin \theta_2) H, \\ \tau_z = (F_1 \sin \theta_1 - F_2 \sin \theta_2) D/2. \end{cases} \quad (1)$$

F_1 , F_2 , θ_1 , and θ_2 represent the thrust generated by the two rotors and the angle between them and the z^B axis, as shown in Fig. 4. The inertial frame (x^I, y^I, z^I) and body frame (x^B, y^B, z^B) are defined. Throughout the paper, the superscripts I and B will be used to denote the inertial and body frame, respectively. The inertial frame follows the convention of North-East-Down (NED). The dynamics of the aerial mode adhere to a standard rigid motion model:

$$\begin{bmatrix} m\mathbf{I} & 0 \\ 0 & \mathbf{J}^B \end{bmatrix} \begin{bmatrix} \dot{v}^I \\ \dot{\Omega}^B \end{bmatrix} + \begin{bmatrix} 0 \\ \hat{\Omega}^B \mathbf{J}^B \Omega^B \end{bmatrix} = \begin{bmatrix} \mathbf{f}_g \\ 0 \end{bmatrix} + \begin{bmatrix} \mathbf{R} \mathbf{f}_F^B \\ \boldsymbol{\tau}^B \end{bmatrix}, \quad (2)$$

$$\mathbf{R} = \mathbf{R}_z(\kappa) \mathbf{R}_y(\omega) \mathbf{R}_x(\varphi). \quad (3)$$

in Eq. 2 and 3, the variables m , \mathbf{I} , and \mathbf{J}^B represent the mass, the identity matrix in $\mathbb{R}^{3 \times 3}$, and the inertia matrix, respectively. The angular velocity vector Ω^B is represented in the body frame, while $\hat{\Omega}^B$ is the skew-symmetric cross

product matrix of Ω^B . The velocity vector v^I is represented in the inertial frame. The gravity vector $f_g = [0 \ 0 \ mg]^T$ represents gravity in the inertial frame. The rotation matrix R transforms from the inertial frame to the body frame, following the Z-Y-X Tait-Bryan order, where κ , ω , and φ represent the yaw, pitch, and roll Euler angles, respectively. The moment vector produced by the rotors in the body frame is denoted as $\tau^B = [\tau_x \ \tau_y \ \tau_z]^T$, where τ_x , τ_y , and τ_z are detailed in Eq. 1. The force vector $f_F^B = [0 \ 0 \ F]^T$, where $F = F_1 \cos \theta_1 + F_2 \cos \theta_2$.

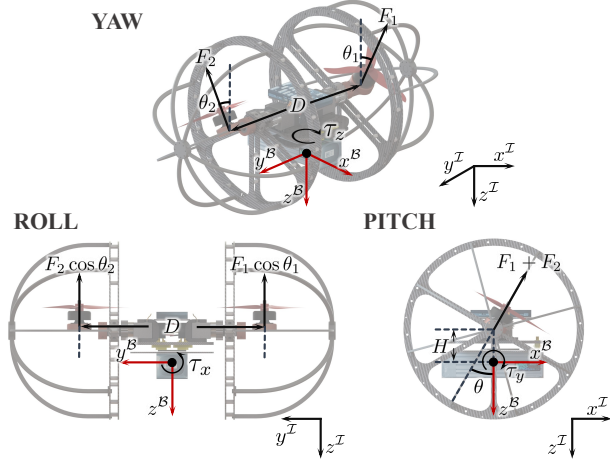


Fig. 4: Dynamic model.

2) **CONTROL**: The control structure of the aerial mode is depicted in Fig. 5. The remote control generates the desired attitude, denoted as q_d , and the force along the body's Z axis, referred to as F_d . The attitude controller calculates the desired moment, τ_d^B , using the desired attitude. Finally, the mixer determines the motor thrust commands and servo angle commands based on τ_d^B and F_d .

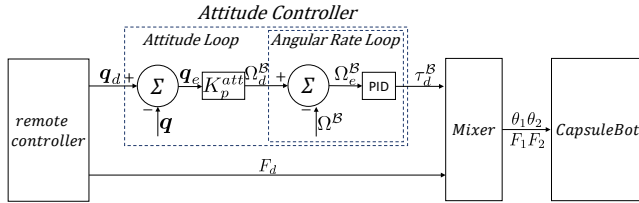


Fig. 5: Control structure of aerial mode.

Attitude Controller: The attitude controller is a cascaded controller consisting of an outer loop, referred to as the angular loop. This loop utilizes a proportional controller to track the desired attitude q_d . The attitude is represented using a quaternion ($q = [\eta, \epsilon]$), where ϵ and η represent the vector and scalar parts of the quaternion, respectively. The quaternion representation enables the calculation of the attitude error q_e and the desired angular velocity Ω_d^B using the ‘‘Quaternion linear’’ method described in [19]:

$$q_e = q_d^* \otimes q = [\eta_e \epsilon_e^T]^T, \quad (4)$$

$$\varphi = 2 \cdot \text{atan2}(\|\epsilon_e\|, \eta_e), \quad (5)$$

$$\Omega_d^B = K_p^{att} \cdot q_e^B = K_p^{att} \cdot \text{sign}(\eta_e) \frac{\varphi}{\sin(\frac{\varphi}{2})} \epsilon. \quad (6)$$

the desired attitude and actual attitude are represented by q_d and q , respectively. The gain from attitude error q_e^B to desired angular velocity Ω_d^B is denoted as K_p^{att} . The inner loop, also known as the angular rate loop, utilizes a PID controller (Eq. 7 and 8) to track the desired angular velocity Ω_d^B :

$$\Omega_e^B = \Omega_d^B - \Omega^B, \quad (7)$$

$$\tau_d^B = K_p^{rt} \cdot \Omega_e^B + K_i^{rt} \cdot \int \Omega_e^B + K_d^{rt} \cdot \dot{\Omega}_e^B. \quad (8)$$

the error in angular velocity and the current angular velocity are denoted as Ω_e^B and Ω^B , respectively. The gains of the PID terms are represented by K_p^{rt} , K_i^{rt} , and K_d^{rt} . The output of the inner loop is the desired moment $\tau_d^B = [\tau_{xd} \ \tau_{yd} \ \tau_{zd}]^T$.

Mixer: The relationship between moments (τ_x, τ_y, τ_z), body-Z force (F), and actuator output ($\theta_1, \theta_2, F_1, F_2$) is illustrated in Fig. 5:

$$\begin{bmatrix} 0 & 1 & 0 & 1 \\ 0 & D/2 & 0 & -D/2 \\ H & 0 & H & 0 \\ D/2 & 0 & -D/2 & 0 \end{bmatrix} \begin{bmatrix} F_1 \sin \theta_1 \\ F_1 \cos \theta_1 \\ F_2 \sin \theta_2 \\ F_2 \cos \theta_2 \end{bmatrix} = \begin{bmatrix} F \\ \tau_x \\ \tau_y \\ \tau_z \end{bmatrix}. \quad (9)$$

Given the desired moments $\tau_d^B = [\tau_{xd}, \tau_{yd}, \tau_{zd}]^T$ and the desired body-Z force F_d , the actuator outputs θ_1, θ_2 , and the rotor thrust outputs F_1, F_2 can be solved from Eq. 9 as follows:

$$\begin{cases} \theta_1 = \text{atan} \left(\frac{D \cdot \tau_{yd} + 2 \cdot H \cdot \tau_{zd}}{H \cdot D \cdot F_d + 2 \cdot H \cdot \tau_{xd}} \right), \\ \theta_2 = \text{atan} \left(\frac{D \cdot \tau_{yd} - 2 \cdot H \cdot \tau_{zd}}{H \cdot D \cdot F_d - 2 \cdot H \cdot \tau_{xd}} \right), \\ F_1 = \frac{1}{2} \cdot \sqrt{\left(\frac{\tau_{yd}}{H} + \frac{\tau_{zd}}{D/2} \right)^2 + \left(F_d + \frac{\tau_{zd}}{D/2} \right)^2}, \\ F_2 = \frac{1}{2} \cdot \sqrt{\left(\frac{\tau_{yd}}{H} - \frac{\tau_{zd}}{D/2} \right)^2 + \left(F_d - \frac{\tau_{zd}}{D/2} \right)^2}. \end{cases} \quad (10)$$

B. Ground Mode

CapsuleBot's control scheme in ground mode is similar to that of a balance bot. It employs a cascade PID controller, with the outer loop tracking the desired velocity along the body's x -axis and the inner loop tracking the desired pitch angle of the robot [20] [21].

$$\begin{cases} \delta_e = K_v^{whl} (v_d - v) - \delta, \\ \omega_{whl1} = K_p^{whl} \delta_e + K_i^{whl} \int \delta_e + K_d^{whl} \dot{\delta}_e - K_\gamma^{whl} (\omega_{\gamma d} - \dot{\gamma}), \\ \omega_{whl2} = K_p^{whl} \delta_e + K_i^{whl} \int \delta_e + K_d^{whl} \dot{\delta}_e + K_\gamma^{whl} (\omega_{\gamma d} - \dot{\gamma}). \end{cases} \quad (11)$$

the variables δ , v_d , v , $\omega_{\gamma d}$, and $\dot{\gamma}$ represent actual values of the pitch angle under ground mode, the expected and actual values of the vehicle velocity, and the steer (yaw) rate, respectively. The gain of the velocity control loop is denoted as K_v^{whl} , and the inner loop PID terms are defined as K_p^{whl} , K_i^{whl} , K_d^{whl} , and K_γ^{whl} . Additionally, ω_{whl1} and ω_{whl2} represent the angular velocity applied by the motors on the wheels.

IV. EXPERIMENTAL VALIDATION

Fig. 1 showcases the platform used for conducting real-world experiments. The SNDWAY sound level monitor sw-525g is used to measure the noise produced by the machine during its operation. This instrument has a measurement range of 30 - 130 dB and is capable of recording noise decibels on the computer at a rate of one measurement per second.

A. Power Consumption

In this experiment, our main objective was to evaluate the energy consumption of CapsuleBot. Specifically, the robot is programmed to roll with a normal angular velocity and a circular trajectory radius of 1 m in a clockwise direction. The aerial mode of the robot is tested while it is connected to the flight control test rack, with the throttle manually maneuvered to 50% to 55%. We allowed the vehicle to run for an extended period of time under these conditions, during which we collected data on energy consumption.

The power of aerial mode, denoted as P_a , is 691.4 W (460.9 W/kg), while the power of ground mode, denoted as P_g , is 4.5 W (3 W/kg). Therefore, we can refer to the work [22] to calculate the power efficiency:

$$\eta = \left(1 - \frac{P_g}{P_a}\right) \times 100\% = 99.35\%. \quad (12)$$

We compare the average power consumption of CapsuleBot with three aerial-ground robots using the bi-copter configuration: DoubleBee [21], SytaB [10] and a single passive wheel-based robot [23]. Figure 6 shows the power consumption in different modes.

In ground mode, the power consumption is very low at approximately 4.5 W (3 W/kg), and CapsuleBot has the lowest energy consumption and highest power efficiency. In aerial mode, the power consumption of CapsuleBot is not as energy-efficient as the others, possibly due to the spherical propeller protector and the structure of the ground mode. These structures affect the airflow and increase the weight of the machine.

B. Noise level

Two series of experiments were conducted to evaluate the noise performance in the ground mode and aerial mode.

In the first series of experiments, as shown in Fig. 7 (a) and (b), the robot starts in an idle state and is programmed to move using a two-wheel differential speed. The sound level monitor is positioned at the center of the circular path, where the wheels rotate at a radius of approximately 1 m . Data collection is continuous throughout the experiment, the specific experimental data can be seen in Fig. 8, with recorded values ranging from a minimum of 49.1 dB to a maximum of 57.4 dB , and an average of 52.42 dB . It is important to note that the ambient noise level when the robot is not in motion is approximately 44.89 dB . Additionally, the noise generated from the motion of the outer wheel, which is approximately 5 m away, averaged 46.28 dB .

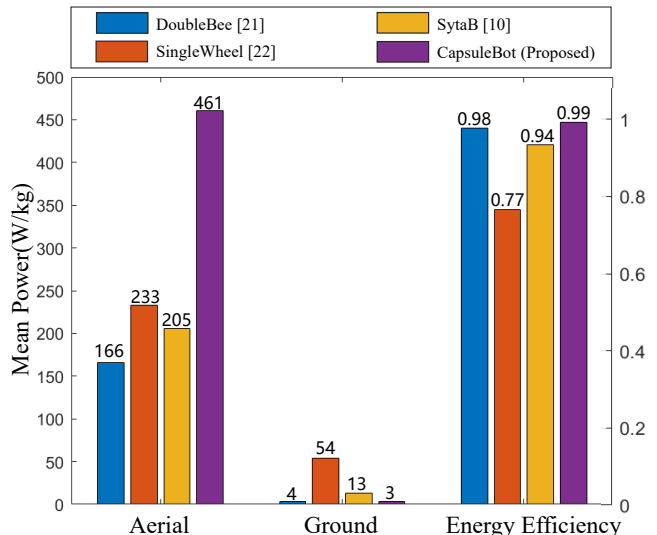


Fig. 6: Comparative analysis of average energy consumption is conducted concerning aerial-ground robots that operate in a bi-copter configuration. The average power consumption data for the DoubleBee is sourced directly from [21], while information pertaining to the SingleWheel can be found in [23]. As for the SytaB, its power consumption is estimated based on visual data extracted from a figure presented in [10].

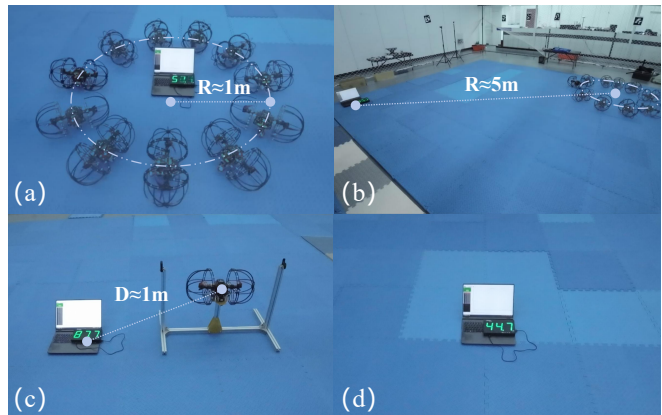


Fig. 7: Real-world experiments of noise level. (a): ground mode noise (1 m), (b): ground mode noise (5 m), (c): aerial mode noise (1 m), (d): ambient noise.

In the second series of experiments, the robot is connected to the flight control test rack. It begins in an idle state and is manually maneuvered to maintain the throttle at 50% to 55%. The robot is positioned approximately 1 m away from the sound level monitor. In this throttle situation, the robot's thrust and noise can simulate the actual aerial mode. This experimental condition allows for maintaining a safer distance (1 m) and experimental operability. Throughout the entire duration of the experiment, the instrument consistently records data, capturing values that range from a minimum of 87.4 dB to a maximum of 89.4 dB , with an average of 88.14 dB .

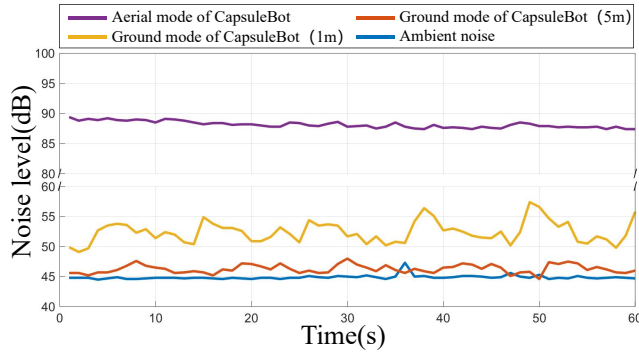


Fig. 8: Results of noise level experiments.

The experimental results, shown in Fig. 8, indicate that the noise level of CapsuleBot in ground mode increases by only 16.77% compared to the ambient noise, decreases by 40.53% compared to the aerial mode (1m). The sound produced by the robot during ground operation is barely audible at a distance of 5 m and is not significantly different from ambient noise. These findings emphasize the benefits of CapsuleBot in terms of quiet operation and highlight its potential for covert reconnaissance applications.

C. Challenging Tasks

To further verify CapsuleBot’s aerial and ground locomotion capabilities, we conducted two challenging tasks based on the structural characteristics and application prospect of CapsuleBot. The robot was controlled to traverse regions with different types of obstacles.

In the first mission scenario, we designed a narrow space, and the robot successfully sped through a gap in air mode. In the second task scenario, we designed a ground covered with wooden block obstacles (the height is 2 cm), and the robot moved steadily through the area in ground mode.

Fig. 9 illustrates these missions. These complex missions clearly demonstrate CapsuleBot’s capability in aerial and ground locomotion and traverse rough terrain and effectively overcome obstacles.

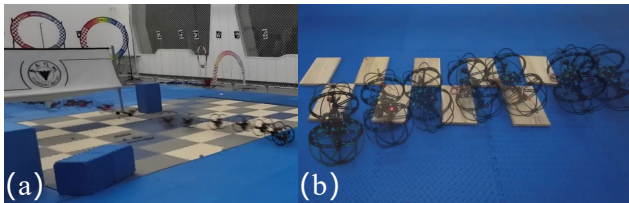


Fig. 9: Real-world experiments of two challenging tasks. (a): aerial mission, (b): ground mission.

D. Benchmark Comparison

In this subsection, we select several hybrid aerial-ground vehicles with different configurations for comparison, representing the design strategies of combination [13], ball wheel [24], deformation [25] and transformation [17] respectively. All above them have the same active-wheel-drive ground

mode and similar application scenarios. We made a comparative analysis according to the corresponding papers, and put forward the following performance indicators.

- (1) Structure simplicity: The evaluation criteria include the additional load and the degree of component reuse of the ground motion mode.
- (2) Energy efficiency: The evaluation criteria include the combined energy consumption and the relative energy savings of the ground mode compared to the flight mode.
- (3) Stealthiness: The evaluation criteria is a comprehensive analysis of the amount of noise and dust generated under the two different motion modes.
- (4) Narrow space trafficability: The evaluation criteria is the ability of the vehicle to move in a small space under the same size.

TABLE I: The Table of the Benchmark

| | Proposed | Tan et al.[13] | Kalantari et al.[22] | Meiri et al.[23] | Zheng et al.[17] |
|-----------------------------|----------|----------------|----------------------|------------------|------------------|
| Structure Simplicity | ★★★★★ | ★ | ★★ | ★★★★ | ★★★★★ |
| Energy Efficiency | ★★★★★ | ★ | ★★ | ★★★★ | ★★★★★ |
| Stealthiness | ★★★★★ | ★★★★ | ★★★★★ | ★ | ★★ |
| Narrow Space Trafficability | ★★★★ | ★ | ★★ | ★★★★ | ★★★★★ |

The result is shown in Tab. I. It is obvious to see that CapsuleBot has an excellent performance in many aspects, while showing minor defections in certain circumstances.

V. CONCLUSION

In conclusion, this paper has introduced CapsuleBot, a compact hybrid aerial-ground vehicle specially engineered for extended covert reconnaissance missions. The innovative design incorporates the aerial maneuverability of a bicopter with the energy-efficient and noise-reducing characteristics of ground vehicles. This synergy is achieved through the development of a unique actuated-wheel-rotor structure, which employs a single motor for both unilateral rotor tilting in bicopter mode and ground movement in terrestrial mode. CapsuleBot features two of these structures, enabling seamless transition between aerial and ground propulsion using only four motors, without the need for additional drivers. Additionally, comprehensive dynamics and control systems have been devised for both aerial and ground mode, leveraging the bicopter and two-wheeled self-balancing vehicle models. Experimental validation has confirmed CapsuleBot’s superior performance, with a remarkable 40.53% reduction in noise and a substantial 99.35% decrease in energy consumption during ground operations. These outcomes underscore the significant potential of CapsuleBot for prolonged covert reconnaissance missions.

In the future, our plan is to optimize the aerodynamics of our robots in order to reduce energy consumption and noise. Additionally, we will focus on optimizing power transmission and control algorithms to enhance control performance.

REFERENCES

- [1] D. Hwang, E. J. Barron III, A. T. Haque, and M. D. Bartlett, "Shape morphing mechanical metamaterials through reversible plasticity," *Science robotics*, vol. 7, no. 63, p. eabg2171, 2022.
- [2] D. Falanga, K. Kleber, S. Mintchev, D. Floreano, and D. Scaramuzza, "The foldable drone: A morphing quadrotor that can squeeze and fly," *IEEE Robotics and Automation Letters*, vol. 4, no. 2, pp. 209–216, 2018.
- [3] K. Mohammadi, S. Sirouspour, and A. Grivani, "Control of multiple quad-copters with a cable-suspended payload subject to disturbances," *IEEE/ASME Transactions on Mechatronics*, vol. 25, no. 4, pp. 1709–1718, 2020.
- [4] W. R. Roderick, M. R. Cutkosky, and D. Lentink, "Bird-inspired dynamic grasping and perching in arboreal environments," *Science Robotics*, vol. 6, no. 61, p. eabj7562, 2021.
- [5] K. Sugihara, M. Zhao, T. Nishio, T. Makabe, K. Okada, and M. Inaba, "Design and control of a small humanoid equipped with flight unit and wheels for multimodal locomotion," *IEEE Robotics and Automation Letters*, 2023.
- [6] B. L. Digney and S. G. Penzes, "Robotic concepts for urban operations," in *Unmanned Ground Vehicle Technology IV*, vol. 4715, pp. 63–74, SPIE, 2002.
- [7] K. L. Cook, "The silent force multiplier: The history and role of uavs in warfare," in *2007 IEEE Aerospace Conference*, pp. 1–7, IEEE, 2007.
- [8] R. Zhang, Y. Wu, L. Zhang, C. Xu, and F. Gao, "Autonomous and adaptive navigation for terrestrial-aerial bimodal vehicles," *IEEE Robotics and Automation Letters*, vol. 7, no. 2, pp. 3008–3015, 2022.
- [9] H. Jia, R. Ding, K. Dong, S. Bai, and P. Chirarattananon, "Quadrolltor: A reconfigurable quadrotor with controlled rolling and turning," *IEEE Robotics and Automation Letters*, 2023.
- [10] J. Yang, Y. Zhu, L. Zhang, Y. Dong, and Y. Ding, "Sytab: A class of smooth-transition hybrid terrestrial/aerial bicopters," *IEEE Robotics and Automation Letters*, vol. 7, no. 4, pp. 9199–9206, 2022.
- [11] K. Kim, P. Spieler, E.-S. Lupu, A. Ramezani, and S.-J. Chung, "A bipedal walking robot that can fly, slackline, and skateboard," *Science Robotics*, vol. 6, no. 59, p. eabf8136, 2021.
- [12] Y. Mulgaonkar, B. Araki, J.-s. Koh, L. Guerrero-Bonilla, D. M. Aukes, A. Makineni, M. T. Tolley, D. Rus, R. J. Wood, and V. Kumar, "The flying monkey: A mesoscale robot that can run, fly, and grasp," in *2016 IEEE international conference on robotics and automation (ICRA)*, pp. 4672–4679, IEEE, 2016.
- [13] Q. Tan, X. Zhang, H. Liu, S. Jiao, M. Zhou, and J. Li, "Multimodal dynamics analysis and control for amphibious fly-drive vehicle," *IEEE/ASME Transactions on Mechatronics*, vol. 26, no. 2, pp. 621–632, 2021.
- [14] J. Hu, Y. Liang, and X. Diao, "A flying-insect-inspired hybrid robot for disaster exploration," in *2017 IEEE international conference on robotics and biomimetics (ROBIO)*, pp. 270–275, IEEE, 2017.
- [15] A. Fabris, E. Aucone, and S. Mintchev, "Crash 2 squash: An autonomous drone for the traversal of narrow passageways," *Advanced Intelligent Systems*, vol. 4, no. 11, p. 2200113, 2022.
- [16] S. Mintchev and D. Floreano, "A multi-modal hovering and terrestrial robot with adaptive morphology," in *Proceedings of the 2nd International Symposium on Aerial Robotics*, no. CONF, 2018.
- [17] Z. Zheng, J. Wang, Y. Wu, Q. Cai, H. Yu, R. Zhang, J. Tu, J. Meng, G. Lu, and F. Gao, "Roller-quadrotor: A novel hybrid terrestrial/aerial quadrotor with unicycle-driven and rotor-assisted turning," *arXiv preprint arXiv:2303.00668*, 2023.
- [18] Y. Qin, W. Xu, A. Lee, and F. Zhang, "Gemini: A compact yet efficient bi-copter uav for indoor applications," *IEEE Robotics and Automation Letters*, vol. 5, no. 2, pp. 3213–3220, 2020.
- [19] X. Lyu, H. Gu, J. Zhou, Z. Li, S. Shen, and F. Zhang, "A hierarchical control approach for a quadrotor tail-sitter vtol uav and experimental verification," in *2017 IEEE/RSJ International Conference on Intelligent Robots and Systems (IROS)*, pp. 5135–5141, IEEE, 2017.
- [20] E. Philip and S. Golluri, "Implementation of an autonomous self-balancing robot using cascaded pid strategy," in *2020 6th International Conference on Control, Automation and Robotics (ICCAR)*, pp. 74–79, 2020.
- [21] M. Cao, X. Xu, S. Yuan, K. Cao, K. Liu, and L. Xie, "Doublebee: A hybrid aerial-ground robot with two active wheels," *arXiv preprint arXiv:2303.05075*, 2023.
- [22] N. Pan, J. Jiang, R. Zhang, C. Xu, and F. Gao, "Skywalker: A compact and agile air-ground omnidirectional vehicle," *IEEE Robotics and Automation Letters*, vol. 8, no. 5, pp. 2534–2541, 2023.
- [23] Y. Qin, Y. Li, X. Wei, and F. Zhang, "Hybrid aerial-ground locomotion with a single passive wheel," in *2020 IEEE/RSJ International Conference on Intelligent Robots and Systems (IROS)*, pp. 1371–1376, IEEE, 2020.
- [24] A. Kalantari, T. Touma, L. Kim, R. Jitosh, K. Strickland, B. T. Lopez, and A.-A. Agha-Mohammadi, "Drivocopter: A concept hybrid aerial/ground vehicle for long-endurance mobility," in *2020 IEEE Aerospace Conference*, pp. 1–10, IEEE, 2020.
- [25] N. Meiri and D. Zarrouk, "Flying star, a hybrid crawling and flying sprawl tuned robot," in *2019 International Conference on Robotics and Automation (ICRA)*, pp. 5302–5308, IEEE, 2019.